Letters in Applied NanoBioScience
Open-Access Journal (ISSN: 2284-6808)

Article
Volume 12, Issue 4, 2023, 131
https://doi.org/10.33263/LIANBS124.131

Molecular Docking and Dynamic Simulation Studies of Cu(II) Metal Complexes with Covid-19 main Protease

Shroff R. Kumaraswamy [1], Kudigana J. Pampa [2], Shivashankrappa Nagashree [3], Puttaswamappa Mallu [3], Vivek Chandramohan [4], Lokanath N. Krishnappagowda [5,*]

[1] Department of Physics, Maharani's Science College for Women, Mysuru-570005, India
[2] Department of Biotechnology, University of Mysore, Manasagangotri, Mysuru-570 006, Karnataka, India
[3] Department of Chemistry, SJCE, JSS Science and Technology University, Mysuru-570 006, Karnataka, India
[4] Department of Biotechnology, Siddaganga Institute of Technology, Tumakuru-572 101, Karnataka, India
[5] Department of Studies in Physics, University of Mysore, Manasagangotri, Mysuru-570 006, Karnataka, India
* Correspondence: lokanatha@physics.uni-mysore.ac.in (N.K.L);

Scopus Author ID: (N.K.L) 57193406019
Received: 12.01.2022; Accepted: 12.03.2022; Published: 18.09.2022

Abstract: Although the vaccine against the COVID-19 pandemic has been achieved, therapeutics still have to design to treat the infected patients. Several studies by the scientific communities are involved all over the world to develop a novel therapeutic agent against the COVID-19 virus. This study screened four β-diketone-based Cu(II) complexes against COVID-19 main protease to study their potential as an antiviral drug molecule. A molecular docking study revealed the excellent inhibitory activity of Cu(II) complexes with good binding energy values. Molecular dynamics simulation studies were carried out for 50ns to explore the selectivity profiles, conformational stability, and fluctuations of protein-ligand complexes during the simulation. Using DFT calculation, the highest occupied and lowest unoccupied molecular orbitals, electronic properties, and molecular electrostatic potential were investigated and compared with the docking results.

Keywords: β-diketone Cu(II) complexes; Sars-CoV-2; molecular docking and dynamics.

1. Introduction

On March 12, 2020, the World Health Organization (WHO) declared Covid-19 an emerging disease [1-3]. COVID-19 is a positive-stranded RNA virus with a crown-like appearance under an electron microscope [4]. Two replicate polyproteins, pp1a and pp1ab are synthesized in the cell when the COVID-19 virus infects it [4,5]. A replication/transcription complex has several structural proteins, and two proteases constitute these polyproteins. One of these proteases is the main protease of coronavirus, which cuts the polyproteins into individual functional pieces, leading to the replication of new viruses [6-8]. Since it mediates viral transcription and replication, the main protease is the best-characterized target for SARS-CoV-2. Various groups have reported the crystal structure main protease with and without the inhibitor [9-12]. Finding suitable inhibitors of the main protease can prevent the COVID-19 virus from multiplying in the host cell. Hence, blocking this enzyme's activity would inhibit viral transcription and replication, which will help design newer drugs [13-14].

In continuation of our previous research work, we have selected beta-diketone Cu(II) complexes such as, 1-phenyl-1,3-butanedione copper(II) complex (M1), 4,4,4-trifluoro-1-phenylbutane-1,3-dione copper(II) complex (M2), 4,4,4-trifluoro-1-(thiophen-2-yl)butane-1,3-

dione copper(II) complex (M3) and 4,4,4-trifluoro-1-(2-naphthyl)-1,3-butanedione copper(II) complex (M4) to investigate their inhibition property against COVID-19 main protease using *in-silico* molecular docking and then molecular dynamics simulation studies. Copper (II) is used in various biological processes, including electron transport and catalysis, and is typically found in enzyme and protein active sites; however, it has been related to the treatment of a variety of diseases, including cancer. The selected Cu(II) complexes showed good antibacterial properties against Methicillin-resistant Staphylococcus aureus (MRSA) bacteria [15-17]. In this study, our attempt is to check their antiviral property against the main protease of the COVID-19 virus. The molecular docking (MD) approach includes several approaches for evaluating drug candidates' bioactivity, physicochemical properties, and pharmacokinetic properties. MD is a powerful approach for structure-based drug discovery (SBDD) [18-22].

This can be used to model the interaction between a small molecule and a protein at the atomic level, which allows to characterization of the behavior of small molecules in the binding site of target proteins and elucidate fundamental biochemical processes [23-31]. We choose the crystal structure of 6LU7 [32] for our study from the PDB, which consists of 312 amino acids. The X-ray crystal structure of 6LU7 is the first deposited main protease structure of the novel COVID-19 which serves as a potential target for the inhibition of COVID-19 [33]. Protease inhibitors are compounds that block the action of proteases and can be used as antiviral drugs.

2. Materials and Methods

2.1. DFT calculations.

DFT calculations were carried out for selected β-diketone copper complexes to optimize the coordinates of the structures. DFT calculations provide identical results to the realistic models of target molecules and also help study the interactions between the receptors and the ligands [34, 35]. The optimization of coordinates of copper complexes was carried out using Gaussian 16 program package [36], using the B3LYP density function with the LanL2DZ basis set for metal atoms and the 6-311+G(d,p) basis set for C, O, F, N, and H atoms. All DFT calculations were visualized using GaussView 5.0.8 [37]. The calculated parameters utilized in this study comprise the Highest Occupied Molecular Orbital (HOMO) and the Lowest Unoccupied Molecular Orbital (LUMO) energies, orbital energy gap, absolute hardness, electronegativity, chemical potential, global softness, and electrophile index. These parameters play a prominent role in explaining the ligands interaction in the binding pocket of COVID-19 main protease. The Molecular Electrostatic Potential surfaces (MEPs) were accomplished from the calculations and visualized using Gauss View.

2.2. Molecular docking studies.

To investigate the effect of selected β-diketone copper complexes with the COVID-19 main protease protein, molecular docking analysis was carried out. MGL tools 1.5.6 [38] with AutoDock Vina [39,40] were used for the molecular docking analysis to detect the preferred binding sites. Crystallographic information files of selected β-diketone copper complexes were used for the ligand preparation by MGL tools 1.5.6. The selected copper complex structures were prepared, optimized and energy minimized.

From the Protein Data Bank, a 3-D structure of the main protease (PDB ID:6LU7) was downloaded in PDB format. The initial preparation of the protein structure was performed by removing water and N3 inhibitor using Biovia Discovery Studio 2019 visualizer [41]. Then

using AutoDock Tools, nonpolar hydrogen atoms were added, and energy was minimized to the main protease. The atomic potential binding site was defined using grid size of x = -11.575, y = 14.611 and z = 65.164. The binding affinity of copper complexes was evaluated in kcal/mole and was found to be negative. Biovia Discovery Studio 2019 visualizer was used to visualize and analyze ligand interactions.

2.3. Molecular dynamics simulation.

Molecular dynamics simulation for 6LU7-M1, M2, M3, and M4 complexes was performed using the Desmond program 30 in Schrödinger suite 2017-2. Protein-ligand complexes were solvated individually in an explicit water box of size 10 using the TIP3P water model with periodic boundary conditions and a simple point charge (SPC) water model [42]. Na^+ or Cl^- ions were added to neutralize the system's total charge, and the NPT ensemble was used to minimize and relax the system with a recording period of 200 ps; each simulation was run for a total of 50 ns. The system was gradually annealed throughout the simulations to maintain a temperature (300 K) and pressure using the Nose-Hoover thermostatic algorithm and the Martina-Tobias-Klein method [43,44]. The simulation interaction diagram tool included in the Desmond package was used to analyze the complete communications between the ligands and protein. The simulation interaction diagram (SID) program in Schrodinger was used to analyze the results in terms of protein and ligand root mean square deviations (RMSD), root mean square fluctuation (RMSF), and protein-ligand interaction fingerprints.

3. Results and Discussion

3.1. Density functional theory calculation.

DFT calculations for selected β-diketone copper complexes M1, M2, M3, and M4 were carried out to compute the LUMO and HOMO orbital energy gap (ΔEgap), electronegativity (χ), chemical potential (μ), global softness (σ), absolute hardness (η) and electrophile index (ω) values (Table 1) which often play governing roles in molecular systems. Figure 1 shows the optimized molecular structures of M1, M2, M3, and M4, as well as the HOMO and LUMO electron density distributions of the Cu(II) complexes. A higher HOMO value shows that a molecule is more likely to transfer its freely bound electron to the suitable orbitals of an acceptor molecule. The decreasing order of HOMO of the Cu(II) metal complexes is M3>M4>M1>M2 it indicates that the M3 complex has a strong preference for donating its most energetic electron to an acceptor molecule's appropriate orbital. The LUMO is a measure of a molecule's tendency to accept electrons from a donor species' proper orbital. The lower the LUMO value, the more likely the molecule is to accept an electron. The values of the LUMO for the studied complexes are in the order M1>M3>M2>M1; the M1 has the highest tendency for accepting electrons from an electron-donating species' appropriately occupied orbitals. The molecular orbital energy gap at the frontier is frequently used as a reactivity or stability indices. M2 complex showed the lowest ΔEgap (Figure 1 and Table 2) among the other Cu(II) complexes. The lower energy gap value makes the flow of electrons easier, so the molecule becomes soft and more reactive. The negative values of chemical potential (μ) for all the Cu(II) complexes indicate good stability, leading to the formation of a stable complex with the receptor. M2 exhibits the lowest hardness values (η) among the selected Cu(II) complexes associated with molecular docking.

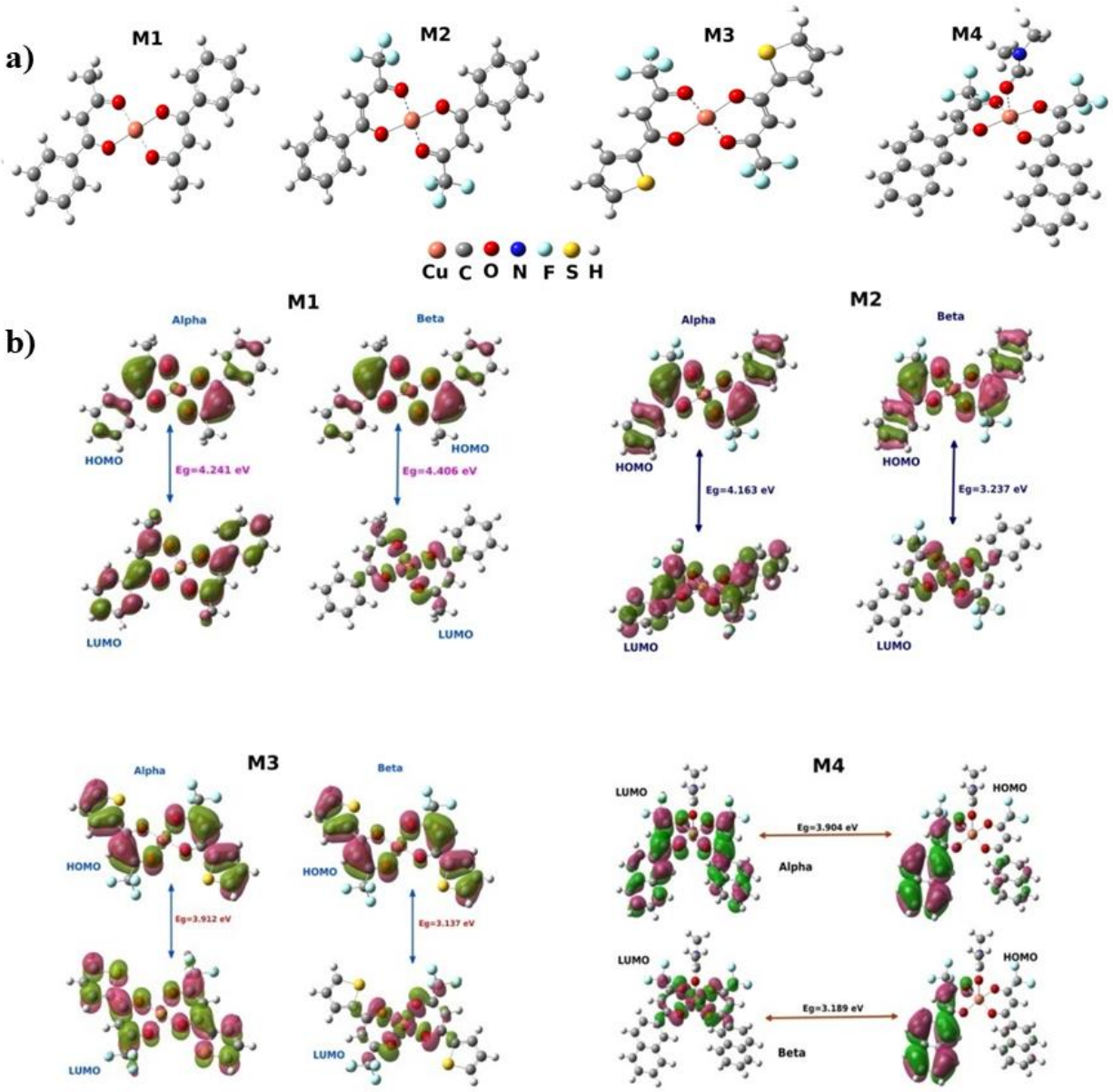

Figure 1. (**a)** Optimised molecular structures; (**b)** Frontier Kohn-Sham molecular orbitals of selected β-diketone copper complexes M1, M2, M3, and M4.

Table 1. Global and local reactive descriptors of selected β-diketone copper complexes M1, M2, M3, and M4.

β-diketone copper complexes		E_{HOMO} (eV)	E_{LUMO} (eV)	ΔE_{gap} (eV)	χ (eV)	η (eV)	σ (eV)	μ (eV-1)	ω (eV)
M1	**Alpha**	-6.231	-1.986	4.241	4.108	2.125	0.470	-4.108	3.969
	Beta	-4.406	-5.904	2.838	4.371	1.533	0.652	-4.371	6.237
M2	**Alpha**	-6.262	-3.136	3.127	4.698	1.563	0.639	-4.698	7.058
	Beta	-4.259	-2.135	2.123	3.197	1.061	0.941	-3.197	4.814
M3	**Alpha**	-7.017	-3.105	3.912	5.061	1.956	0.512	-5.061	6.547
	Beta	-6.974	-3.837	3.137	5.406	1.568	0.637	-5.406	9.316
M4	**Alpha**	-6.187	-2.198	3.989	4.192	1.194	0.501	-4.192	3.390
	Beta	-6.170	-2.851	3.319	4.510	1.659	0.600	-4.510	2.821

3.2. Molecular docking results.

Since no therapeutic agents are available for treating infection caused by the covid-19, only several FDA-approved drugs [45], anti-HIV, and anti Malarial drugs are offered as supportive actions to treat the infection [46-53]. In this work, we study the efficiency of β-diketone Cu(II) complexes as inhibitors against the main protease of SARS-CoV-2 proteins. Molecular docking analysis is a preliminary way to screen the potential drug candidates for a specific disease in less time. The results obtained from the docking studies have shown that the Cu(II) complexes bind in the active site of the main protease of a covid-19 virus. A summary of the results obtained from docking of studied β-diketone Cu(II) complexes with main protease (PDB:6LU7) is summarized in Table 2.

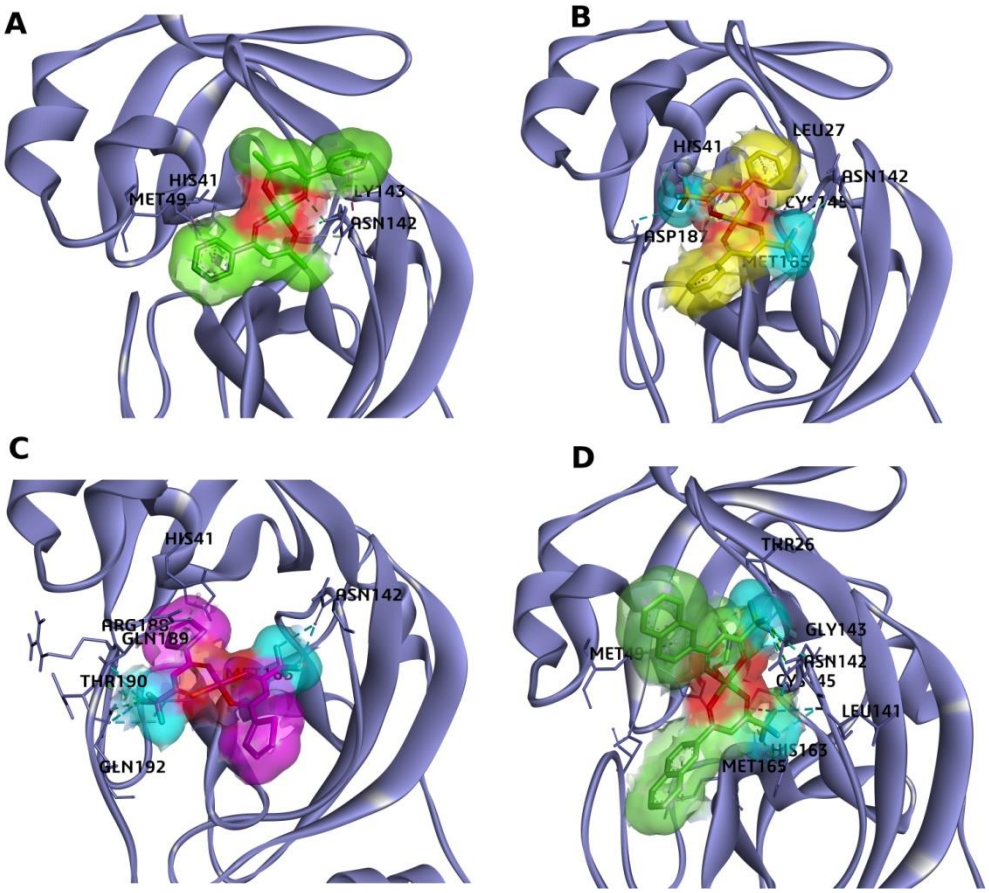

Figure 2. Glide Docking. Predicted binding mode of M1, M2, M3, and M4 in a main protease of Covid-19. Close-up view of the main protease active site (PDB ID: 6LU7). The protein is rendered with ribbons, and key residues are shown as sticks. The docked poses of **(A)** M1**, (B)** M2, **(C)** M3; **(D)** M4**.**

3.2.1. Interaction of M1 with the main protease.

The interaction of M1 with the main protease showed good affinity and the ligand fitted inside the binding pocket region of the protease (Figure 2A) with the binding energy -8.1 kcal/mol. The most important interaction between M1 and the protein is described by two hydrogen bonding between NH and bridging carbon group of residue ASN142 and coordinating oxygen atoms of M1 at a distance of 2.32, 2.47, and 3.60 Å, respectively (Table 2 and Figure 3a). Figure 3a represents the H-bond profile between M1 and main protease, clearly showing that ASN142, GLY143, and HIS141 act as hydrogen donor residues, whereas MET49 is a hydrogen acceptor residue. The benzene ring of the M1 complex is active by making π-carbon interaction with the imidazole ring of HIS41 residue with a distance of

4.30 Å. Apart from these interactions, π-alkyl, and amide-π stacked interaction bonds are formed by the residue MET49 and GLY143 with the benzene ring of M1 (Figure 3a and Table 2).

3.2.2. Interaction of M2 with the main protease:

M2 is bound to the active pocket of the main protease (Figure 2B) with a greater binding energy of -9.5 kcal/mol. Fluorine atom and benzene π system of the M2 complex bind to the catalytic dyad (CYS-145 and HIS-41) of the main protease with strong conventional hydrogen (3.54 Å) and π-anion (4.48 Å) bonds. The significant interactions between M2 and the main protease are portrayed by two hydrogen bond interactions between NH groups of GLU166 and HIS163 with chelating oxygen and fluorine atoms of M2. Main protease-M2 binding is also stabilized by π-sulfur, π-stacked, and fluorine interactions between MET165, MET149, HIS41, THR190, GLN189 residues, and π system of the benzene ring and fluorine atoms of the M2 (Figure 3b and Table 2). Figure signifies the H-bonds between M2 and main protease. Amino acid residues CYS145, GLU166, HIS41, and HIS163, are active as hydrogen donors, whereas MET165, MET149, and THR190 as hydrogen acceptor residues (Figure 3b and Table2).

3.2.3. Interaction of M3 with the main protease:

The binding affinity of M3 with the main protease is explored with the energy value -9.5 kcal/mol. Fluorine groups of the M3 showed an excellent binding affinity towards the main protease with strong H-bond and hydrophobic interactions (Figure 2C and 3c). NH and NH2 groups of THR190 and GLN192 amide residues formed two strong conventional hydrogen bonds with the donor-acceptor distance of 2.71 and 2.83 Å, respectively. C=O moiety of THR190 and ASN142 attached to the M3 with three and two fluorine bond interactions, respectively. Hydrophobic interaction between MET165 and HIS41 residues and centroid of the thiophene ring of M3 is observed with a distance of 4.43 and 4.97 Å, respectively (Figure 3c and Table 2). Figure 3 clearly demonstrates the hydrogen donor and acceptor amino acid residues with pink and green colors.

3.2.4. Interaction of M4 with the main protease:

With binding energy of -8.8 kcal/mol, the copper complex M4 fitted inside the active site of the main protease, exploring five-strong H-bond and hydrophobic interactions (Figure 2D). HIS166, ASN142, and HLY143 amino acid residues act as hydrogen donors to form strong H-bonds with the fluorine group of M4, whereas THR26, MET49, and LEU141 are active as hydrogen acceptor residues. Hydrophobic interactions between sulfur of CYS145 and fluorine atoms of M4 played a significant role in protein-ligand complex stability. The peptide group of THR126 and LEU141 residues interact with the fluorine and carbon atoms of M4. Also, MET49 and MET165 residues form the π-alkyl bonds with the π system of naphthalene rings of M4, contributing to the stability of the main protease-M4 complex (Figure 3d and Table 2).

3.3. Molecular dynamic simulation.

The Molecular dynamic simulation study was carried out for copper complexes for further analysis of molecular docking results. To assess the binding stability of the main protease, docked complexes with β-diketone Cu(II) complexes (M1, M2, M3, and M4) were

subjected to a simulation study for a 50 ns simulation period in the binding region of the main protease. To examine dynamic behavior throughout the simulation period, all the protein-ligand complexes were analyzed by the calculation of RMSD, RMSF, and Protein-ligand interactions.

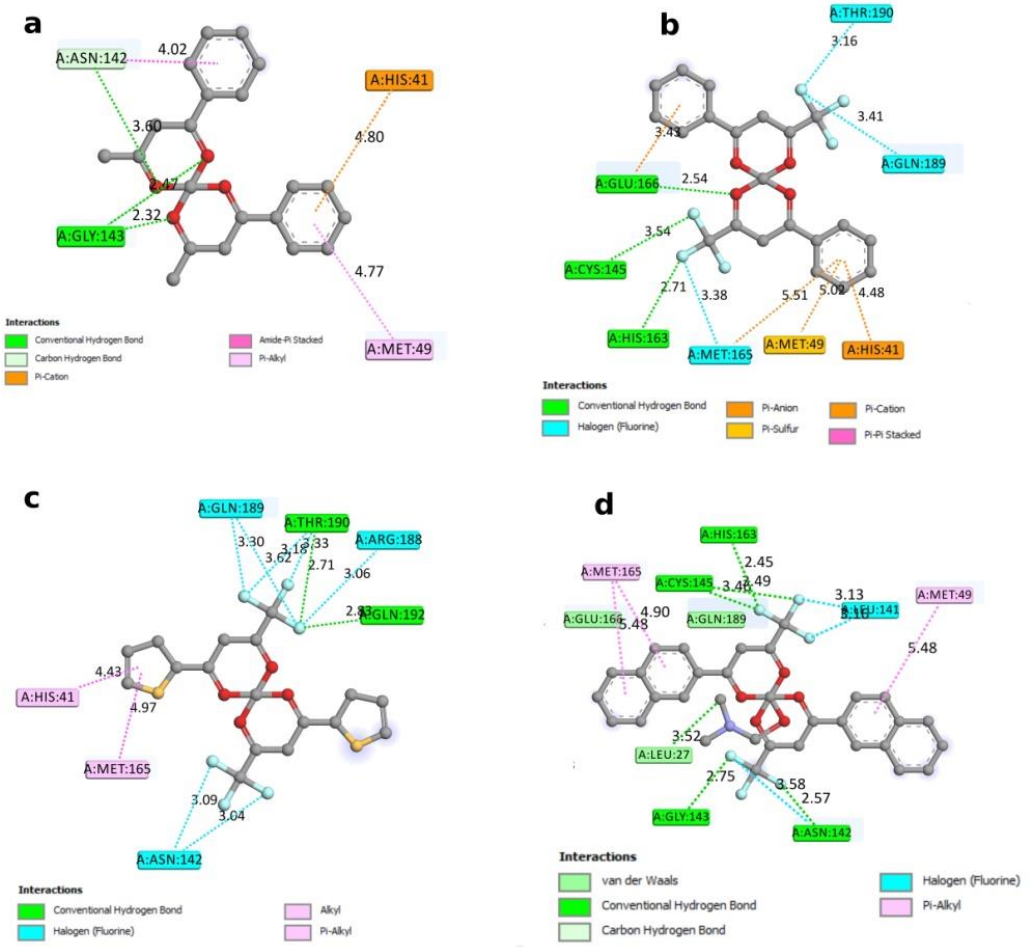

Figure 3. 2D interactions between main protease and copper complexes **(a)** M1; **(b)** M2, **(c)** M3; **(d)** M4.

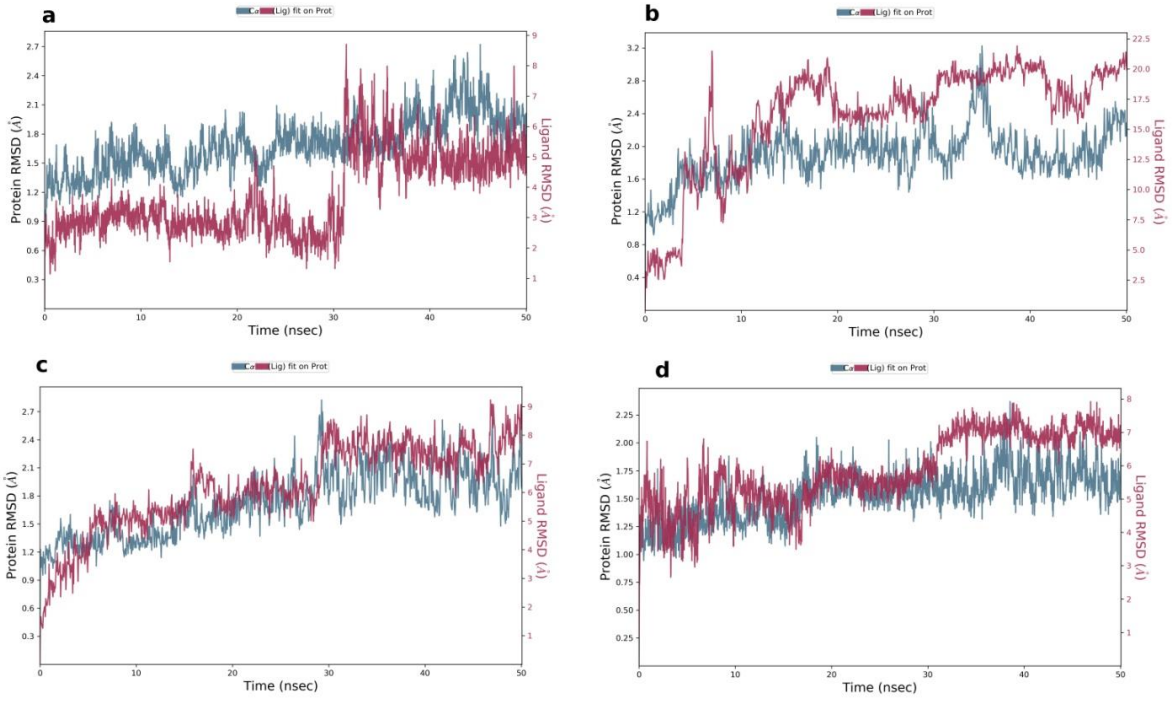

Figure 4. RMSD profiles of the complexes **(a)** M1; **(b)** M2; **(c)** M3; **(d)** M4 during the MD simulations.

3.3.1. Root mean square deviation (RMSD).

MSD fluctuations of the all protein-ligand complex were examined during the 50ns MD simulation to measure the equilibration, protein flexibility, conformational changes, and translational and rotational movements inside the protease binding site. Figure 4 depicts the RMSD plot for all four ligands and protein backbone RMSD. The selected molecules remain stable throughout the simulation within the acceptable range of change in backbone RMSD. Molecules M1 and M4 showed good stability, as these molecules are equilibrated at 0ns, remain stable till 30ns, then fluctuated by ~0.75 and ~0.25 Å, respectively, after they remained stable throughout the molecular simulation. The ligand RMSD for the M3 molecule fluctuates from 0.45 Å to 1.9 Å till 30ns then reaches 2.3 Å and stabilizes till 50 ns. The oscillations in the RMSD values for the studied complexes indicated the durability of hydrogen and other bond interactions and showed these molecules are more active inside the binding pocket of the main protease. The detailed insight into the RMSD of all the selected ligands and main proteases is depicted in Figure 4.

3.3.2. Root mean square fluctuation (RMSF.

RMSF for protein-ligand complexes was measured based on the fluctuations at the residue level. To explore more insight into the protein flexibility, the time average of RMSF values of the 300 amino acids of covid 19 main protease with the presence of M1, M2, M3, and M4 molecules over the simulation period were calculated. RMSF plots of all four molecules indicate that binding to the receptor was stable and showed a minor effect on the flexibility of the protein throughout the simulation period. The RMSF values for the 6LU7-M4 complex stabled with fewer fluctuations among the other three complexes. The maximum fluctuation in the RMSF graph of the 6LU7-M4 complex was observed in the residue CYS300 with the RMSF value of 2.75 ± 0.08 Å. The active site residues (LEU141, ASN142, GLY143, HIS163, and MET165), which contributed to the protein-ligand binding, showed fewer fluctuations. The RMSF values for the 6LU7-M1, M2, and M3 complexes indicated that the residues TYR37, CYS38, PRO39, ALA206, VAL204, and LEU205, showed less fluctuation during the simulation period with the average RMSF values of the residues ~ 0.36 ± 0.04, 0.30 ± 0.06, and 0.43 ± 0.06 Å respectively.

3.3.3. Protein-Ligand Contacts.

Fingerprints of ligands interaction in the active site of the protein are shown in Figure 5. In 6LU7-M4 and 6LU7-M1 complexes, ASN142 establishes hydrogen bonds with 74 and 31% of the simulation time, respectively. 6LU7-M1 complex SER144 and GLY143 exhibit the hydrogen-bonded interactions mediated by a water molecule with 62 and 42% of the simulation period, respectively (Figure 5). In the 6LU7-M3 complex, GLN189 and GLU166 residues maintain the hydrogen bonds and water bridges which help to maintain overall ligand stability during simulation GLU166, THR26, and ASN142 are the most prevalent ligand interactions in the binding sites of all four complexes. While the remaining ligand interacts with the protein of amino acids in the complex, as shown in Figure 6.

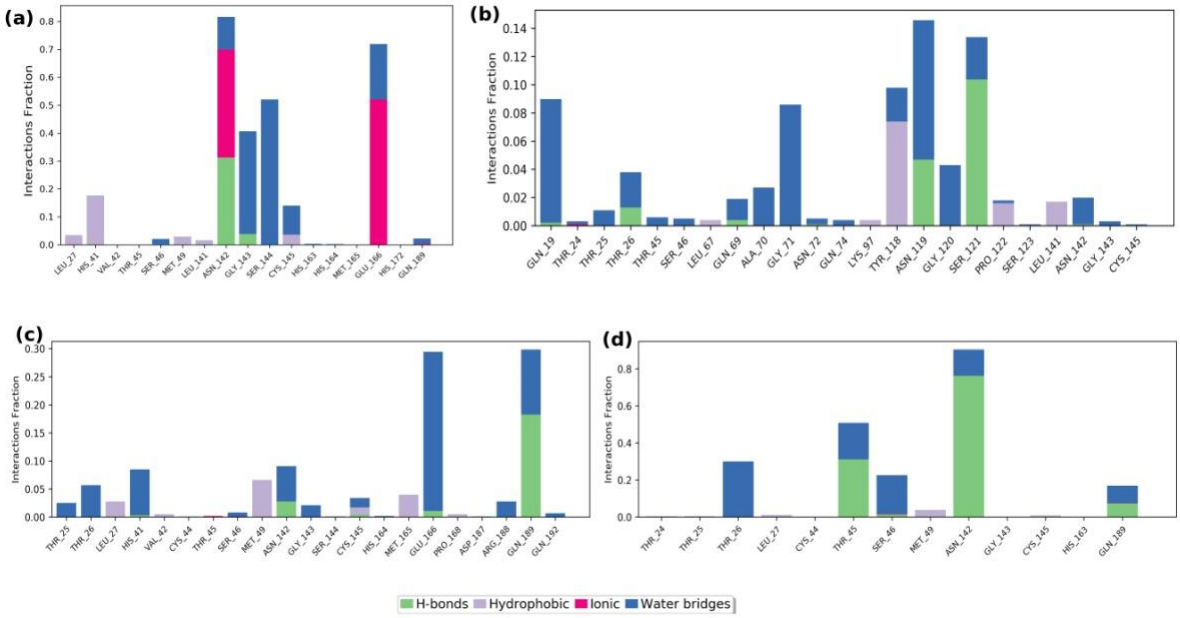

Figure 5. Fingerprints of protein-ligand interactions during the MD simulations where in **(a)** M1; **(b)** M2; **(c)** M3; **(d)** M4**.**

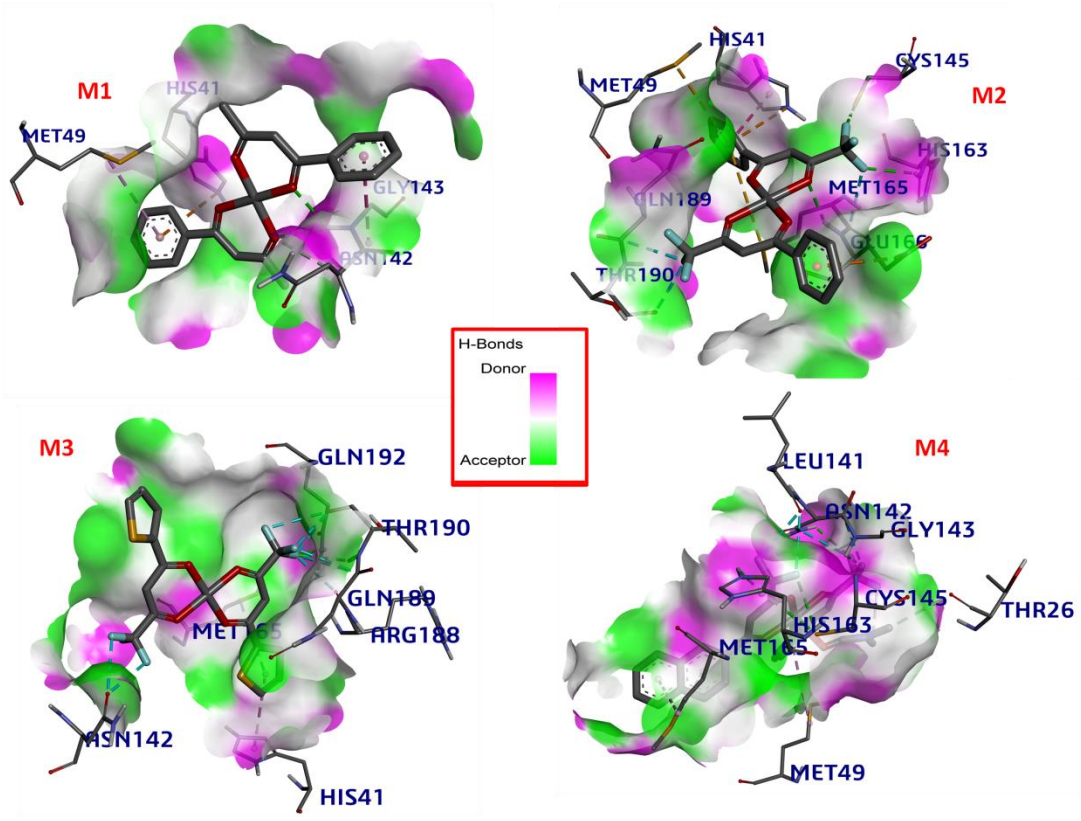

Figure 7. H-bond profile of the complexes **(a)** M1; **(b)**M2; **(c)** M3; **(d)** M4 during the MD simulations.

Table 2. Glide docking interaction details between main protease and selected ligands.

M1	GLY143	O1	Conventional	2.32
	GLY143	O2	Conventional	2.47
	ASN142	O1	Carbon	3.60
	MET49	Centroid of the benzene	π Alkyl	4.77
	HIS41	Centroid of the benzene	π Cation	4.80
M2	GLU166	N	Conventional	2.54

	HIS163	F1	Conventional Fluorine	2.71
	THR190	F3	Fluorine	3.16
	GLU166	C	Fluorine	3.38
	THR190	C	Fluorine	3.41
	GLU166	Centroid of the benzene	π Anion	3.43
	CYS145	F2	Conventional Fluorine	3.54
	HIS41	Centroid of the benzene	π π Stacked	4.22
	HIS41	Centroid of the benzene	Pi Cation	4.48
	MET49	Centroid of the benzene	Sulfur	5.02
	MET165	Centroid of the benzene	Pi sulfur	5.51
M3	THR190	N	Conventional; Fluorine	2.71
	THR190	0	Fluorine	2.72
	GLN192	F5	Conventional; Fluorine	2.83
	ASN142	F2	Fluorine	3.04
	GLN189	O	Fluorine	3.06
	ASN142	F5	Fluorine	3.09
	THR190	O	Fluorine	3.18
	GLN189	F2	Fluorine	3.30
	THR190	O	Fluorine	3.33
	GLN189	F5	Fluorine	3.62
	HIS41	Centroid of the benzene	Pi Alkyl	4.43
	MET165	Centroid of the benzene	Alkyl	4.97
M4	HIS163	F4	Conventional; Fluorine	2.45
	ASN142	FOA	Conventional; Fluorine	2.57
	GLY143	F2	Conventional; Fluorine	2.75
	LEU141	F6	Fluorine	3.13
	LEU141	F1	Fluorine	3.16
	HIS163	F4	Conventional; Fluorine	3.46
	CYS145	F6	Conventional; Fluorine	3.49
	THR26	C1	Corbon	3.50
	ASN142	FOA	Conventional; Fluorine	3.57
	ASN142	F3	Fluorine	3.58
	MET165	Centroid of the benzene	Pi Alkyl	4.90
	MET165	Centroid of the benzene	Pi Alkyl	5.48
	MET48	Centroid of the benzene	Pi Alkyl	5.48

4. Conclusions

In the present research work, selected β-diketone Cu(II) complexes were studied against covid-19 main protease to test their potential as an antiviral agent. The compounds were subjected to theoretical studies, and their optimized molecular structure and FMO images were obtained by the DFT-B3LYP method at 6311++G(d,p). Molecular docking analysis showed the significant inhibitory activity of Cu(II) complexes with the binding energy values of -8.1, -9.5, -9.5, and -8.8 kcal/mol for M1, M2, M3, and M4, respectively. These inhibitors interact with the catalytic dyad in the active site of the COVID-19 main protease, which is vital in viral replication. All four complexes were subjected to molecular dynamics simulation studies to confirm the stability of protein-ligand complexes structure during the simulation period of

50ns. The top 1 hit compound (M3) showed excellent binding energy, the highest hydrogen bond occupancy, and an excellent range of RMSD and RMSF values for 6LU7 protein. It's calculated HOMO-LUMO energy gap is 3.91 and 3.13ev for alpha and beta. The study provides the basic foundation for the -diketone-based Cu(II) complexes to be used as potential inhibitors in regulating main protease function and controlling viral replication. Further, its potential can be proved by its *in-vivo*, *in-vitro*, and clinical studies.

Funding

This research was funded by SJCE, JSS Science and Technology University, and VGSTCISEE Project (GRD 647), GOK, Karnataka

Acknowledgments

The authors are thankful to SJCE, JSS Science and Technology University, and VGST-CISEE Project (GRD 647), GOK, Karnataka.

Conflicts of Interest

The authors declare no conflict of interest.

References

1. Brandon, Havranek.; Shahidul, M. Islam. An in silico approach for identification of novel inhibitors as potential therapeutics targeting COVID-19main protease. *J. Biomol. Struct. Dyn* **2020**, *39*, 4304-4315, https://doi.org/10.1080/07391102.2020.1776158.
2. Bheenaveni, R.S. India's indigenous idea of herd immunity: the solution for COVID-19. *Tradit. Med. Res* **2020,** *5*, 182–187, https://search.bvsalud.org/global-literature-on-novel-coronavirus-2019-ncov/resource/en/covidwho-618724.
3. Dong, E.; Du, H.; Gardner, L. An interactive web-based dashboard to track COVID-19inrealtime.*LancetInfect.Dis*. **2020**, *20*, 533–534, https://doi.org/10.1016/S1473-3099(20)30120-1.
4. Fehr, A.R.; Perlman, S. Coronaviruses: an overview of their replication and pathogenesis. *Coronaviruses* **2015**, 1-23, https://link.springer.com/protocol/10.1007/978-1-4939-2438-7_1.
5. Ziebuhr, J.; Siddell, S.G. Processing of the human coronavirus 229E replicase polyproteins by the virus-encoded 3C-like proteinase: identification of proteolytic products and cleavage sites common to pp1a and pp1ab. *J. Virol*. **1999**, *73*, 177-185, https://doi.org/10.1128/JVI.73.1.177-185.1999.
6. Thiel, V.; Ivanov, K.A.; Putics, A.; Hertzig, T.; Schelle, B.; Bayer, S.; Ziebuhr, J. Mechanisms and enzymes involved in SARS coronavirus genome expression. *J. Gen. Virol.* **2003**, *84*, 2305-2315, https://doi.org/10.1099/vir.0.19424-0.
7. Snijder, E.J.; Bredenbeek, P. J.; Dobbe, J. C.; Thiel, V.; Ziebuhr, J. Poon, L. L., Gorbalenya, A. E. Unique and conserved features of genome and proteome of SARS-coronavirus, an early split-off from the coronavirus group 2 lineage. *J. Mol. Biol*. **2003**, *331*, 991-1004, https://doi.org/10.1016/S0022-2836(03)00865-9.
8. Ziebuhr, J.; Heusipp, G.; Siddell, S.G. Biosynthesis, purification, and characterization of the human coronavirus 229E 3C-like proteinase. *J. Virol*. **1997**, *71*, 3992-3997, https://doi.org/10.1128/jvi.71.5.3992-3997.1997.
9. Hatada, R.; Okuwaki, K.; Mochizuki, Y.; Handa, Y.; Fukuzawa, K.; Komeiji, Y.; Tanaka, S. Fragment Molecular Orbital Based Interaction Analyses on COVID-19 Main Protease-Inhibitor N3 Complex (PDB ID: 6LU7). *J. Chem. Inf. Model* **2020**, *60*, 3593-3602, https://doi.org/10.1021/acs.jcim.0c00283.
10. Hatada, R.; Okuwaki, K.; Mochizuki, Y.; Handa, Y.; Fukuzawa, K.; Komeiji, Y.; Tanaka, S. Fragment Molecular Orbital Based Interaction Analyses on COVID-19 Main Protease-Inhibitor N3 Complex(PDBID:6LU7) *J.Chem.Inf.Mode***2020**, *60*, 3593-3602, https://doi.org/10.1021/acs.jcim.0c00283.
11. Zhang, L.; Lin, D.; Sun, X.; Curth, U.; Drosten, C.; Sauerhering, L.; Hilgenfeld, R.. Crystal structure of SARS-CoV-2 main protease provides a basis for design of improved α-ketoamide inhibitors. *Science* **2020**, *368*, 409-412, https://doi.org/10.1126/science.abb3405.

12. Yang, S.; Chen, S.J.; Hsu, M.F.; Wu, J.D.; Tseng, C.T.K.; Liu, Y.F.; Hsu, M.C. Synthesis, crystal structure, structure− activity relationships, and antiviral activity of a potent SARS coronavirus 3CL protease inhibitor. J. Med. Chem **2006**, *49*, 4971-4980, https://doi.org/10.1021/jm0603926.
13. Chen, S.; Hu, T.; Zhang, J.; Chen, J.; Chen, K.; Ding, J.; Shen, X. Mutation of Gly-11 on the dimer interface results in the complete crystallographic dimer dissociation of severe acute respiratory syndrome coronavirus 3C-like protease: crystal structure with molecular dynamics simulations. *Int. J. Biol. Chem* **2008**, *283*, 554-564, https://doi.org/10.1074/jbc.M705240200.
14. Hegyi, A.; Ziebuhr, J. Conservation of substrate specificities among coronavirus main proteases. *J. Gen. Virol* **2002**, *83*, 595-599, https://doi.org/10.1099/0022-1317-83-3-595.
15. Krishnegowda, H.M.; Karthik, C.S.; Marichannegowda, M.H.; Kumara, K.; Kudigana, P.J.; Lingappa, M.; Neratur, L.K. Synthesis and structural studies of 1-phenyl-1, 3-butanedione copper (II) complexes as an excellent antimicrobial agent against methicillin-resistant Staphylococcus aureus. *Inorganica Chimica Acta* **2019**, *484*, 227-236, https://doi.org/10.1016/j.ica.2018.09.049.
16. Hema, M.K.; Karthik, C.S.; Pampa, K.J.; Manukumar, H.M.; Mallu, P.; Warad, I.; Lokanath, N.K. Solvent induced 4, 4, 4-trifluoro-1-(2-naphthyl)-1, 3-butanedione Cu (II) complexes: Synthesis, structure, DFT calculation and biocidal activity. *Polyhedron* **2019**, *168*, 127-137, https://doi.org/10.1016/j.poly.2019.04.028.
17. Hema, M.K.; Karthik, C.S.; Warad, I.; Lokanath, N.K.; Zarrouk, A.; Kumara, K.; Mallu, P. Regular square planer bis-(4, 4, 4-trifluoro-1-(thiophen-2-yl) butane-1, 3-dione)/copper (II) complex: Trans/cis-DFT isomerization, crystal structure, thermal, solvatochromism, hirshfeld surface and DNA-binding analysis. *J. Mol. Struct* **2018**, *1157*, 69-77, https://doi.org/10.1016/j.molstruc.2017.12.048.
18. Lavecchia, A.; Di Giovanni, C. Virtual screening strategies in drug discovery: a critical review. *Curr. Med. Chem* **2013**, *20*, 2839-2860, https://doi.org/10.2174/09298673113209990001.
19. Meng, X.Y.; Zhang, H.X.; Mezei, M.; Cui, M. Molecular docking: a powerful approach for structure-based drug discovery. *Curr Comput Aided Drug Des* **2011**, *7*, 146-157, https://doi.org/10.2174/157340911795677602.
20. Lengauer, T.; Rarey, M. Computational methods for biomolecular docking. *Curr. Opin. Struct. Biol* **1996**, *6*, 402-406, https://doi.org/10.1016/S0959-440X(96)80061-3.
21. Ferreira, L.G.; Dos Santos, R.N.; Oliva, G.; Andricopulo, A.D. Molecular docking and structure-based drug design strategies. *Molecules* **2015**, *20*, 13384-13421, https://doi.org/10.3390/molecules200713384.
22. De Vivo, M.; Cavalli, A. Recent advances in dynamic docking for drug discovery. Wiley Interdisciplinary Reviews*: Wiley Interdiscip. Rev. Comput. Mol. **Sci* **2017**, *7*, e1320, https://doi.org/10.1002/wcms.1320.
23. Falchi, F.; Caporuscio, F.; Recanatini, M. Structure-based design of small-molecule protein–protein interaction modulators: the story so far. *Future Med. Chem* **2014**, *6*, 343-357, https://doi.org/10.4155/fmc.13.204.
24. M. Salah.; M.E. Belghiti.; A.O. Aitouna.; A. Zeroual.; S. Jorio.; H. El Alaoui Abdellaoui.; H. El Hadki.; K. Marakchi.; N. Komiha,.MEDT Study of the 1,3-DC Reaction of Diazomethane with Psilostachyin and investigation about the interactions of some pyrazoline derivatives with Protease (Mpro) of nCoV-2, *J. Mol. Graph. Model* **2021,***102,*107763, https://doi.org/10.1016/j.jmgm.2020.107763.
25. Anuj Kumar.; Gourav Choudhir.; Sanjeev Kumar Shukla.; Mansi Sharma.; Pankaj Tyagi.; Arvind Bhushan.; Madhu Rathore. Identification of phytochemical inhibitors against main protease of COVID-19 using molecular modeling approaches. *J. Biomol. Struct. Dyn.* **2020**, https://doi.org/10.1080/07391102.2020.1772112.
26. Jordaan, M.A.; Ebenezer, O.; Damoyi, N.; Shapi, M. Virtual screening, molecular docking studies and DFT calculations of FDA approved compounds similar to the non-nucleoside reverse transcriptase inhibitor (NNRTI) efavirenz. *Heliyon* **2020**, *6*, e04642, https://doi.org/10.1016/j.heliyon.2020.e04642.
27. Jibin, K.; Varughese, K.L.; Joseph Libin, K.S.; Sindhu, A.V.; Rosily.; T.G. Abi . Investigation of the inhibitory activity of some dietary bioactive flavonoids against SARSCoV- using molecular dynamics simulations and MM-PBSA calculations, *J. Biomol. Struct. Dyn* **2021**, https://doi.org/10.1080/07391102.2021.1891139.
28. Ranabir Majumder.; Mahitosh Mandal. Screening of plant-based natural compounds as a potential COVID-19 main protease inhibitor: an insilico docking and molecular dynamics simulation approach, *J. Biomol. Struct. Dyn* **2020**, https://doi.org/10.1080/07391102.2020.1817787.
29. Durgesh Kumar.; Kamlesh Kumari.; Abhilash Jayaraj.; Vinod Kumar.; Ramappa Venkatesh Kumar.; Sujata K. Dass.; Ramesh Chandra.; Prashant Singh . Understanding the binding affinity of noscapines with protease

of SARS-CoV-2 for COVID-19 using MD simulations at different temperatures, *J. Biomol. Struct. Dyn* **2020**,*39*, 2659-2672, https://doi.org/10.1080/07391102.2020.1752310.
30. Kalirajan Rajagopal.; Potlapati Varakumar.; Baliwada Aparna.; Gowramma Byran.; Srikanth Jupudi. Identification of some novel oxazine substituted 9-anilinoacridines as SARS-CoV-2 inhibitors for COVID-19 by molecular docking, free energy calculation and molecular dynamics studies, *J. Biomol. Struct. Dyn* **2020**,*39*,5551-5562, https://doi.org/10.1080/07391102.2020.1798285.
31. Papia Chowdhury. In silico investigation of phytoconstituents from Indian medicinal herb 'Tinosporacordifolia (giloy)' against SARS-CoV-2 (COVID-19) by molecular dynamics approach, *J. Biomol. Struct. Dyn* **2020**,*39*,6792-6809, https://doi.org/10.1080/07391102.2020.1803968.
32. Anoop Kallingal.; Varun Thachan Kundil.; Aravind Ayyolath.; Abraham Peele Karlapudi.; Tomy Muringayil Joseph.; Jayadevi Variyar E. Molecular modeling study of tectoquinone and acteoside from Tectonagrandis linn: a new SARS-CoV-2 main protease inhibitor against COVID-19, *J. Biomol. Struct. Dyn* **2020**, https://doi.org/10.1080/07391102.2020.1832580.
33. Liu, X.; Zhang, B.; Jin, Z.; Yang, H.; Rao, Z. The crystal structure of COVID-19 main protease in complex with an inhibitor N3. *Protein DataBank* **2020**, http://doi.org/10.2210/pdb6LU7/pdb.
34. Gurumallappa.; Arun Renganathan, R.R.; Hema, M.K.; Karthik, C.S.; Rani, S.; Nethaji, M.; Jayanth, H.S.; Mallu, P.; Lokanath, N.K.; Ravishankar Rai V. 4-acetamido-3-nitrobenzoic acid-structural, quantum chemical studies, ADMET and molecular docking studies of SARS-CoV2. J. Biomol. *Struct. Dyn* **2021**, 1-15, https://doi.org/10.1080/07391102.2021.1889664.
35. Hema, M.K.; Karthik, C.S.; Pampa, K.J.; Mallu, P.; Lokanath N.K. 4, 4, 4-trifluoro-1-phenylbutane-1, 3-dione metal [Cu (II) and Ni (II)] complexes as an superlative antibacterial agent against MRSA: Synthesis, structural quantum-chemical and molecular docking studies. *J. Mol. Struct* **2021**, *1243*, 130774, https://doi.org/10.1016/j.molstruc.2021.130774.
36. Frisch M.J.; Trucks G.W.; Schlegel H.B.; Scuseria G.E.; Robb M.A.; Cheeseman J.R.; Li X. *Gaussian* **2016,** *16*,
37. Dennington R.D.; Keith T.A.; Millam J.M. *GaussView* **2016,** 6.0.16.
38. Gurumallappa G.; Jayashankar J.; Puttaswamy A.; Sunderraj J.; Mallu P.; Beeregowda K. 4-(tert-butyl)-N, N-diethylbenzenesulfonamide: Structural, absorption distribution metabolism excretion toxicity (ADMET) and molecular docking studies. *Curr. Chem. Lett* **2021**, *10*, 329-336, http://dx.doi.org/10.5267/j.ccl.2021.3.004.
39. Nanjundaswamy, S.; Jayashankar, J.; Chethana, M.H.; Renganathan, R.A.; Karthik, C.S.; Ananda, A.P.; Nagashree, S.; Mallu, P.; Rai V.R. Design, Synthesis, and In-silico Studies of Pyrazolylpyridine Analogues: A Futuristic Antibacterial Contender against Coagulase Positive Superbug-MRSA. *J. Mol. Struct* **2022**, 132400, https://doi.org/10.1016/j.molstruc.2022.132400.
40. Huey, R..; Morris, G.M.; Forli, S. Using AutoDock 4 and AutoDock vina with AutoDockTools: a tutorial. *The Scripps Research Institute Molecular Graphics Laboratory* **2012**, *10550*, 92037-1000, https://www.moodle.is.ed.ac.uk/pluginfile.php/87431/mod_resource/content/1/2012_ADTtut.pdf.
41. Hema, M.K.; ArunRenganathan, R.R.; Nanjundaswamy, S.; Karthik, C.S.; Mohammed, Y.H.I.; Alghamdi, S.; Mallu, P. N-(4-bromobenzylidene)-2, 3-dihydrobenzo [b][1, 4] dioxin-6-amine: Synthesis, crystal structure, docking and in-vitro inhibition of PLA2. *J. Mol. Struct* **2020**, *1218*, 128441, https://doi.org/10.1016/j.molstruc.2020.128441.
42. Jorgensen, W.L.; Chandrasekhar, J.; Madura, J.D.; Impey, R.W.; Klein, M.L. Comparison of simple potential functions for simulating liquid water. *J. Chem. Phys* **1983,** *79*, 926–935, https://doi.org/10.1063/1.445869.
43. Hoover, W.G. Canonical dynamics: equilibriumphase-space distributions. PhysRev ***1981,*** *A31*.1695 https://doi.org/10.1103/PhysRevA.31.1695.
44. Martyna, G.J.; Tobias, D.J.; Klein, M.L. Constant pressure molecular dynamics algorithms. *J. Chem. Phys* **1994**. *101*, 4177–4189, https://doi.org/10.1063/1.467468.
45. Kandeel, M.; Al-Nazawi, M. Virtual screening and repurposing of FDA approved drugs against COVID-19 main protease. *Life Sci* **2020**, *251*, 117627, https://doi.org/10.1016/j.lfs.2020.117627.
46. Gavriatopoulou, M..; Ntanasis-Stathopoulos, I..; Korompoki, E.; Fotiou, D.; Migkou, M.; Tzanninis, I. G.; Dimopoulos, M.A. Emerging treatment strategies for COVID-19 infection. *Clin. Exp. Med* **2020**, 1-13, https://link.springer.com/article/10.1007/s10238-020-00671-y.
47. Popov, D. Treatment of Covid-19 Infection. A rationale for current and future pharmacological approach. EC Pulmonol. *Respir. Med* **2020**, *9*, 38-58, https://www.yourhealthfirst.uk/wp-content/uploads/2020/04/ECPRM-09-00577.pdf.

48. Dixon, D.L.; Van Tassell, B.W.; Vecchié, A.; Bonaventura, A.; Talasaz, A.H.; Kakavand, H.; Abbate, A. Cardiovascular considerations in treating patients with coronavirus disease 2019 (COVID-19*). J. Cardiovasc. Pharmacol* **2020**, https://dx.doi.org/10.1097%2FFJC.0000000000000836.
49. Carafoli, E. Chloroquine and hydroxychloroquine in the prophylaxis and therapy of COVID-19 infection. *Biochem. Biophys. Res. Commun* **2020,***538,*156-162, https://doi.org/10.1016/j.bbrc.2020.09.128.
50. Ong, W.Y.; Go, M.L.; Wang, D.Y.; Cheah, I.K.M.; Halliwell, B. Effects of antimalarial drugs on neuroinflammation-potential use for treatment of COVID-19-related neurologic complications. *Mol. Neurobiol* **2021**, *58*, 106-117, https://link.springer.com/article/10.1007/s12035-020-02093-z.
51. Yamini, R.S.; Bhargavi, R.S.; Bhuvaneswari, K. Drug repositioning in the treatment Of Covid-19. *J Med Pharm Allied Sci* **2020**, *9*, 2412-2417, https://jmpas.com/admin/assets/article_issue/1588518713JMPAS_MARCH_-APRIL_2020.pdf.
52. Varghese, G.M.; John, R.; Manesh, A.; Karthik, R.; Abraham, O.C. Clinical management of COVID-19. *Indian J. Med. Res* **2020**, *151*, 401, https://dx.doi.org/10.4103%2Fijmr.IJMR_957_20.
53. Naghipour, S.; Ghodousi, M.; Rahsepar, S.; Elyasi, S. Repurposing of well-known medications as antivirals: hydroxychloroquine and chloroquine from HIV-1 infection to COVID-19. *Expert Rev. Anti-infect. Ther* **2020**, *18*, 1119-1133, https://doi.org/10.1080/14787210.2020.1792291.